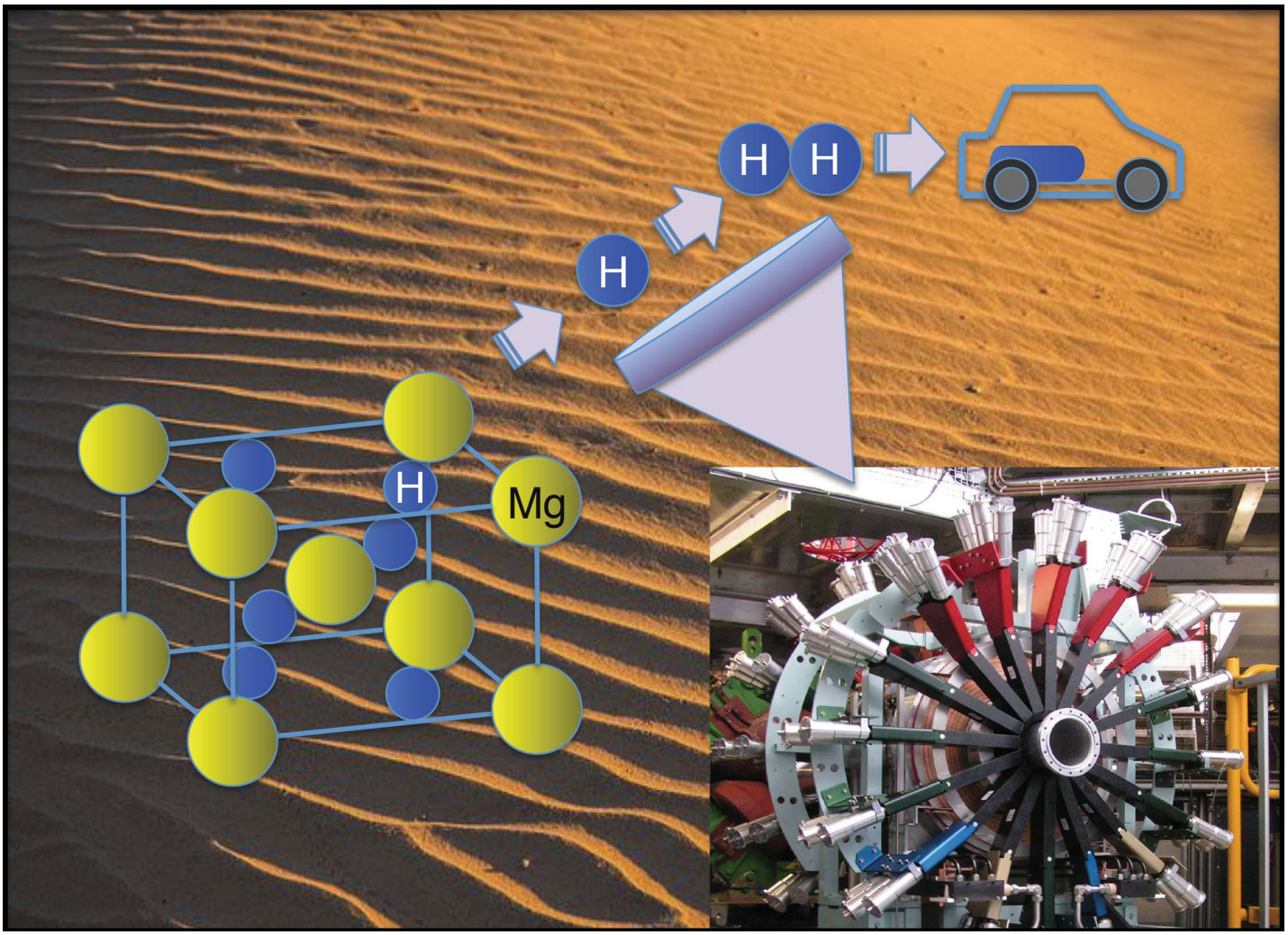

An article presented by Jun Sugiyama *et al.*, Toyota Central Research & Development Laboratories, Inc., Nagakute, Japan.

Desorption reaction in MgH_2 studied with *in situ* μ^+SR

A novel *in situ* muon spin relaxation experiment has been carried out at the ISIS source to investigate mechanisms determining the desorption temperature of hydrogen storage materials. Experiments on MgH_2 reveal the important role of hydrogen diffusion in accelerating the desorption reaction by removing the reaction product, H_2, from the reaction system.

As featured in:

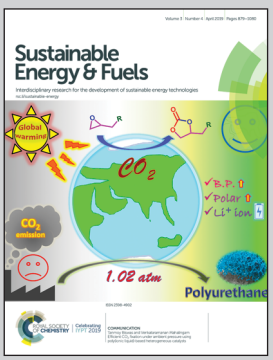

See Jun Sugiyama *et al.*, *Sustainable Energy Fuels*, 2019, **3**, 956.

ROYAL SOCIETY OF CHEMISTRY | Celebrating IYPT 2019

rsc.li/sustainable-energy

Registered charity number: 207890

Sustainable Energy & Fuels

PAPER

View Article Online
View Journal | View Issue

Cite this: *Sustainable Energy Fuels*, 2019, **3**, 956

Desorption reaction in MgH_2 studied with *in situ* μ^+SR

Jun Sugiyama, *[a] Izumi Umegaki,[a] Mitsuru Matsumoto,[a] Kazutoshi Miwa,[a] Hiroshi Nozaki,[a] Yuki Higuchi,[a] Tatsuo Noritake,[a] Ola K. Forslund,[b] Martin Månsson,[b] Stephen P. Cottrell,[c] Akihiro Koda,[d] Eduardo J. Ansaldo[e] and Jess H. Brewer[fg]

Received 22nd November 2018
Accepted 28th January 2019

DOI: 10.1039/c8se00568k

rsc.li/sustainable-energy

In order to study the mechanism determining the desorption temperature (T_d) of hydrogen storage materials, we have measured positive muon spin rotation and relaxation (μ^+SR) in MgH_2 over a wide temperature range including its T_d. The pressure in the sample cell due to desorbed H_2 was measured in parallel with the μ^+SR measurements under static conditions. Such *in situ* μ^+SR measurements revealed that hydrogen starts to diffuse in MgH_2 well below T_d. This indicates the important role of hydrogen diffusion in accelerating the desorption reaction by removing the reaction product, *i.e.* H_2, from the reaction system.

1 Introduction

Positive muon spin rotation and relaxation (μ^+SR) techniques are widely used for studying local magnetic environments in solids[1,2] for both static and dynamic behaviors of the internal magnetic field(s) H_{int} at the muon site(s). However, due to limited counting rates for recording μ^+SR spectra, past μ^+SR measurements were usually performed under fixed conditions, *i.e.* at a constant temperature, pressure and magnetic field. Consequently, it was hitherto impractical to use μ^+SR to study *changes* in H_{int} during chemical reactions of materials.

Recent developments in pulsed muon beams at ISIS in the UK[3] and at J-PARC in Japan,[4] together with the installation of multi-detector counting systems,[5–7] have increased the counting rate to above 100 M events per h. This means that one μ^+SR spectrum with acceptable statistics is recorded within 5–30 minutes. Therefore, if we select a suitable material, μ^+SR can provide information on the *change* in H_{int} during a fairly rapid reaction, in an *in situ* manner. Here we report our first *in situ* μ^+SR study of magnesium hydride, MgH_2 (see Fig. 1), in order to reveal the change in H_{int} during its hydrogen desorption reaction at high temperatures.

An ideal hydrogen storage material is expected to absorb and desorb hydrogen gas reversibly without capacity fading, preferably at room temperature.[9] Magnesium hydride (MgH_2) is known to be one of the promising hydrogen storage materials, because of its relatively low cost and high gravimetric and volumetric hydrogen densities.[10–13] However, its high enthalpy of decomposition leads to a high hydrogen desorption temperature (T_d) and slow reaction rate. Such disadvantages for

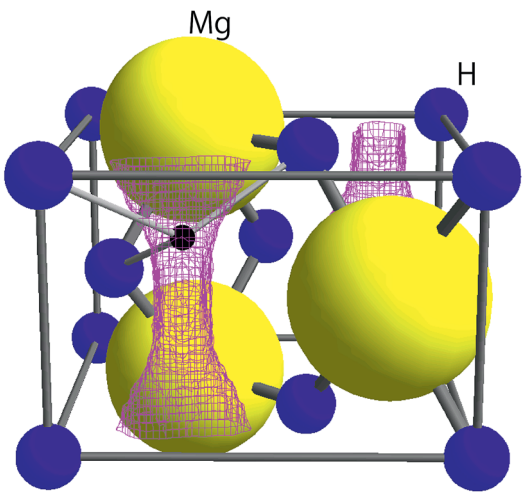

Fig. 1 The crystal structure of MgH_2 in tetragonal symmetry with the space group $P4_2/mnm$ together with the μ^+ sites predicted by DFT calculations (see Section 3.1). The lattice parameters determined from synchrotron radiation powder diffraction data[8] are $a = 4.5198(7)$ Å, $c = 3.0250(6)$ Å, and $V = 61.80$ Å^3. The pink lines represent the iso-surface of potential energy $\phi_E = 600$ meV. A small black sphere represents the muon site, at which ϕ_E shows a local minimum.

[a]*Toyota Central Research & Development Laboratories, Inc., 41-1 Yokomichi, Nagakute, Aichi, 480-1192, Japan. E-mail: e0589@mosk.tytlabs.co.jp; juns@triumf.ca; Fax: +81-561-63-6920; Tel: +81-561-71-8029*

[b]*Department of Applied Physics, KTH Royal Institute of Technology, Electrum 229, SE-16440 Kista, Stockholm, Sweden*

[c]*ISIS Muon Facility, Rutherford Appleton Laboratory, Didcot, Oxfordshire, OX11 0QX UK*

[d]*Muon Laboratory, J-PARC, KEK, Tokai, Ibaraki, 319-1106, Japan*

[e]*Department of Physics & Engineering Physics, University of Saskatchewan, Saskatoon, SK, S7N 5E2 Canada*

[f]*Department of Physics & Astronomy, University of British Columbia, Vancouver, BC, V6T 1Z1 Canada*

[g]*TRIUMF, 4004 Wesbrook Mall, Vancouver, BC, V6T 2A3 Canada*

applications are alleviated significantly by milling[14–16] and by adding catalytic agents, such as Nb_2O_5.[17–20] In fact, the measurements under dynamic conditions, *i.e.* with a temperature programmed desorption (TPD) and/or thermogravimetry (TG) technique, revealed that T_d = 710 K for bulk MgH_2,[21,22] while milling decreases T_d by about 100 K (ref. 21 and 22) and about another 100 K decrease can be achieved by milling together with 5 wt% of Nb_2O_5.[23–25] Such a large decrease in T_d, *i.e.* 200 K in total, and a simple crystal structure make MgH_2 a very attractive model material[11–13] to understand the way to control T_d in storage materials.

Based on macroscopic measurements and numerical calculations, the desorption reaction in MgH_2 is thought to consist of the following five steps under the assumption that a MgH_2 core is surrounded by a Mg shell in each particle:[12,26]

(1) decomposition of MgH_2 at the interface between MgH_2 and Mg;

(2) diffusion of H across the Mg shell;

(3) penetration of H at the surface of the Mg shell;

(4) recombination of chemisorbed H and physisorption;

(5) desorption to the gas phase.

A past quasi-elastic neutron scattering experiment[27] revealed that the diffusion coefficient of hydrogen (D_H) in MgH_2 ranges below 2.5 × 10^{-9} cm^2 s^{-1} even at 650 K, which is lower by at least three orders of magnitude than D_H in Mg (10^{-9} cm^2 s^{-1} at 300 K).[12] Considering the rates of the above five reaction steps, the third and/or fourth steps are thought to be a rate-determining process for the overall desorption reaction,[12,19,26,28] although the nucleation of Mg and formation of the channels by Mg metal nuclei are proposed to be crucial for bulk MgH_2.[29] The hydrogen diffusion in MgH_2 is thus believed to be unessential for the desorption reaction in MgH_2. Nevertheless, a ^{1}H-NMR study on MgH_2,[30] which provides microscopic information of hydrogen dynamics, suggests a faster H motion even at 333 K in milled MgH_2 with Nb_2O_5 than in bulk MgH_2. Indeed, there are still large discrepancies between experimental results and calculated predictions for hydrogen diffusion in MgH_2.[31–36]

We have therefore used μ^+SR to study H_{int} in MgH_2 (where it arises mainly from the nuclear magnetic moment of ^{1}H), since the diffusion coefficients of Li^+ and Na^+ are estimated for many battery materials using the fluctuation rate of H_{int} detected with μ^+SR.[37–46] Due to the fact that the natural abundance of ^{25}Mg with I = 5/2 is 10%, the μ^+SR spectrum caused by the μ^+s stopped in a Mg phase should be time independent, particularly above room temperature. Taking into account a very small concentration of diffusing H in Mg, H diffusion in Mg is invisible with μ^+SR, but such behavior in MgH_2 should be visible. This is because H diffusion enhances the fluctuation rate of H_{int} in MgH_2 formed by ^{1}H. In fact, our previous μ^+SR measurements on MgH_2 (ref. 47 and 48) showed a clear difference in H_{int} among the three MgH_2 samples: as-prepared MgH_2, milled MgH_2, and MgH_2 milled together with 5 wt% of Nb_2O_5. That is, although H_{int} is static up to T_d in the as-prepared sample, H_{int} of the two milled samples becomes dynamic below T_d.

Remembering that μ^+ behaves as a light isotope of H^+ in solids,[1,2] μ^+ is expected to be mobile in any system where H is diffusing, regardless of the charge state of H. However, the differences between the diffusive behaviors observed by μ^+SR in the three MgH_2 samples imply that μ^+ diffusion is *not* equivalent to H diffusion in MgH_2. This naturally motivated us to study the hydrogen desorption reaction in MgH_2 with a more sophisticated μ^+SR experiment, using a combination of an intense muon beam and simultaneous pressure monitoring—namely an *in situ* μ^+SR technique. Here, we report the result of our first attempt to observe the diffusive behavior in MgH_2 with *in situ* μ^+SR.

2 Experimental

2.1 Sample preparation

A powder sample of MgH_2 was purchased from Wako Pure Chemical Industries, Ltd., which will be referred to as ap-MgH_2 in the text. Then 3 g of ap-MgH_2 powder was milled with 300 g stainless steel balls in a stainless steel pot by using a planetary ball mill (Fritsch Japan Co., Ltd, P-5/4) for 24 hours; this sample will be referred to as m-MgH_2 in the text. Then a mixture of 2.85 g of ap-MgH_2 powder and 0.15 g (5 wt%) of Nb_2O_5 powder (Aldrich) was also milled for 24 hours in the same way as the above; this sample will be referred to as mwn-MgH_2 in the text.

2.2 μ^+SR

In order to observe hydrogen dynamics, the μ^+SR spectra were measured in a zero field (ZF), longitudinal field (LF), and transverse field (TF) on the EMU[5] surface muon beam line at the ISIS facility of the Rutherford Appleton Laboratory in the U.K. Here TF (LF) means the magnetic field perpendicular (parallel) to the initial muon spin polarization. The statistics of each spectrum were 40 M events for ZF, 30 M events for LF, and 10 M events for TF with a counting rate of about 80 M events per h. Since the LF-spectra were measured at LF = 5 and 10 Oe, it took about 1.4 hours to obtain the data at one temperature point. Then, the sample was heated to the next temperature at a rate of 1–2 K min^{-1}. The temperature range for the measurements was maintained between 300 and 800 K using a furnace [Fig. 2(a)].

Each sample was sealed in a stainless steel cell (grade 316) with two gold O-rings [Fig. 2(b)] in a He-filled glove box. The window of the cell was also made of stainless steel foil with 50

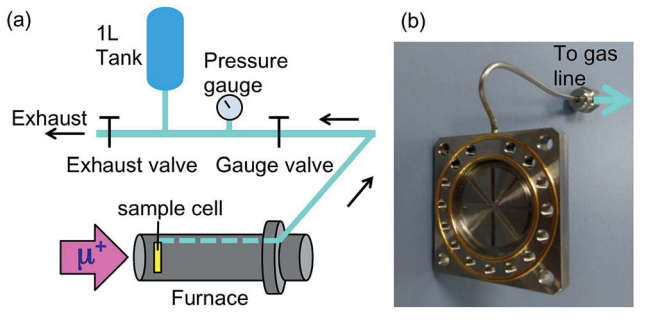

Fig. 2 (a) A schematic illustration of the experimental setup for *in situ* μ^+SR measurements. Hydrogen gas in a sample cell is collected through a gas line equipped with a gas tank and a pressure gauge. (b) The sample cell made of stainless steel with a capillary to collect the liberated gas and gold O-rings for the sealing.

μm thickness. Then the cell was mounted onto the furnace so that the direction of the muon beam is perpendicular to the window. As a result, the muons were implanted into the sample through the window. The released gas was collected through the aforementioned 1/16″ capillary tube, also made from stainless steel, connecting the cell to a one liter tank [Fig. 2(a)]. Before the measurements, the cell, gas line, and tank were evacuated at room temperature, then, the exhaust valve was closed, and then, the sample was heated by the furnace. The total amount of the gas released was determined by measuring the pressure (p) in the gas tank with a Baratron pressure gauge. Prior to the *in situ* experiment at ISIS as explained above, μ^+SR spectra were also measured at both TRIUMF and J-PARC.[47,48] The details of μ^+SR techniques are explained elsewhere.[1,2] The obtained μ^+SR data were analyzed with musrfit.[49]

3 Results

3.1 Predicted muon sites

Knowledge of the site(s) for the implanted μ^+s in the lattice is essential to understanding the μ^+SR data. According to electrostatic potential (E) calculations using a first principles DFT+GGA method, there is likely one shallow E minimum for the implanted μ^+ in the MgH_2 lattice (Fig. 1). However, the distribution of E in the lattice describes a "chimney-shaped" one-dimensional (1D) channel along the c-axis, connecting many local E minima between two neighboring hydrogens, as described in Section 4.1.

The zero-point energy (E_{zero}) of an H atom in solids is typically about 200 meV.[50] Since E_{zero} is approximately scaled by a factor of the inverse of the square root of the mass, E_{zero} for μ^+ is expected to be about 600 meV. The "extended minimum" for E < 600 meV, within which the implanted μ^+ will be located, is illustrated by the region within pink shaded cylinders in Fig. 1. This indicates that the μ^+s will be in a delocalized state within the 1D channel, particularly at high temperatures. It should be noted that we ignored the local lattice distortion due to the implanted μ^+ in the above calculations. Therefore, the observed μ^+SR spectrum is probably either a superposition of multiple spectra from muons at different sites or the signature of a μ^+ in a delocalized quantum state.

3.2 μ^+SR spectra

The ZF-μ^+SR spectrum exhibits a characteristic oscillation for the all three samples below 350 K [Fig. 3(a)], as already reported. This indicates the formation of a collinear three-spin-$\frac{1}{2}$ system (H-μ-H) and a two spin-$\frac{1}{2}$ system (H-μ), as is the case for many hydrogen storage materials.[51,52] The muon spin depolarization function in ZF caused by collinear H-μ-H [$P^{ZF}_{H\mu H}(t)$] is given by[53]

$$P^{ZF}_{H\mu H}(t) = \frac{1}{2} + \frac{1}{6}\cos\left(\sqrt{3}\,\omega_d t\right) + \frac{1+\frac{1}{\sqrt{3}}}{6}\cos\left(\frac{3+\sqrt{3}}{2}\omega_d t\right) + \frac{1-\frac{1}{\sqrt{3}}}{6}\cos\left(\frac{3-\sqrt{3}}{2}\omega_d t\right). \quad (1)$$

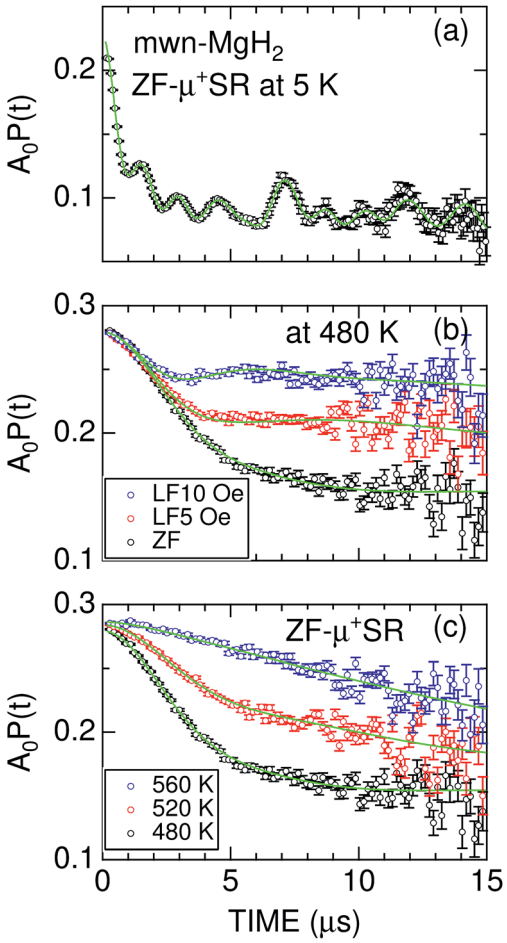

Fig. 3 (a) The ZF-μ^+SR spectrum of mwn-MgH_2 at 5 K; (b) the ZF- and LF-μ^+SR spectra of mwn-MgH_2 at 480 K; and (c) the ZF-μ^+SR spectra of mwn-MgH_2 at 480, 520, and 560 K. In (a), a solid line represents the best fit using a combination of one H-μ-H and eight H-μ signals. In (b) and (c), solid lines represent the best fit obtained using eqn (3). The fitted initial asymmetry is A_0 = 0.24 for (a) and 0.28 for (b) and (c); based on the measurement of a silver reference sample, this means that only a small fraction of the implanted μ^+ form a hydrogen-like muonium (μ^+e^-) state in MgH_2 at 5 K.

On the other hand, $P^{ZF}_{H\mu}(t)$ is given by[54]

$$P^{ZF}_{H\mu}(t) = \frac{1}{6} + \frac{1}{6}\cos(\omega_d t) + \frac{1}{3}\cos\left(\frac{1}{2}\omega_d t\right) + \frac{1}{3}\cos\left(\frac{3}{2}\omega_d t\right). \quad (2)$$

where $\omega_d = 2\pi f_d = (\mu_0\hbar\gamma_\mu\gamma_H)/(4\pi r^3)$, in which μ_0 is the permeability of vacuum, $\hbar$ is the reduced Planck constant, γ_μ is the gyromagnetic ratio of μ^+, γ_H is the nuclear gyromagnetic ratio of ^{1}H, and r is the distance between μ and H in the H-μ-H and H-μ systems.

In fact, the ZF-μ^+SR spectrum was well fitted by a combination of one $P^{ZF}_{H\mu H}(t)$ and eight $P^{ZF}_{H\mu}(t)$ signals, indicating the presence of multiple muon sites in the lattice. Since the fit shows that about 10% of the implanted μ^+s form a H-μ-H state with r = 1.16 Å at 5 K, such muons *sit* at the middle of the two neighboring H^-s. However, the distance between the two nearest neighbor H^-s in the MgH_2 lattice is 3.27 Å.[8] This means that μ^+ attracts the two neighboring H^-s, as in the case for alkali

halides.[53] Considering the presence of the other eight muon sites evidenced by the formation of H-μ systems, the obtained μ^+SR result is very consistent with the predictions from the first principles calculations.

At temperatures above 300 K, the ZF-μ^+SR spectrum clearly shows a Kubo–Toyabe (KT) type relaxation [Fig. 3(b)] due to random nuclear magnetic fields. This means that both H-μ-H and H-μ are no longer stable at high temperatures, because of the thermal vibration of H, being consistent with the findings of ^{1}H-NMR.[55] Since the applied LF = 10 Oe significantly suppresses the relaxation by *decoupling* $H_{\rm int}$,[56] the magnitude of the random nuclear magnetic fields at the muon sites is comparable to the applied LF. This is a typical value for nuclear magnetic fields in solids.[1,2,42]

For both m-MgH_2 and mwn-MgH_2, as temperature increases from 300 K, the KT behavior changes from static to dynamic above around 450 K and finally the relaxation rate becomes very small compared with that at lower temperatures [Fig. 3(c)]. This indicates that the field fluctuation rate (ν) is very rapid compared with the static width (Δ) due to $H_{\rm int}$, as in the case for Li- and Na-diffusion in battery materials.[37–46]

In order to extract Δ and ν from the μ^+SR data for the three samples, the ZF- and LF-μ^+SR spectra were fitted by a combination of two dynamic Gaussian KT signals ($G^{\rm DGKT}$)[57] and a time-independent background signal coming from the muons stopping in the sample cell:

$$A_0P(t) = A_{\rm KT1}G^{\rm DGKT}(\Delta_1, \nu_1, t, H_{\rm LF}) + A_{\rm KT2}G^{\rm DGKT}(\Delta_2, \nu_2, t, H_{\rm LF}) + A_{\rm BG}, \quad (3)$$

where A_0 is the initial ($t = 0$) asymmetry, $A_{{\rm KT}i}$ and $A_{\rm BG}$ are the asymmetries associated with the three signals (the first two from the μ^+ stopped in the sample and the last from those stopped in the sample cell), Δ_i represents the static widths of the local field distributions at the μ^+ sites, and ν_i represents the fluctuation rates of the fields at those sites. For $\nu = 0$ and $H_{\rm LF} = 0$ (*i.e.* ZF), $G^{\rm DGKT}$ (t, Δ, ν, $H_{\rm LF}$) becomes a *static* Gaussian Kubo–Toyabe function,[57] $G_{zz}^{\rm KT}(t, \Delta) = \frac{1}{3} + \frac{2}{3}(1 - \Delta^2t^2)\exp\left(-\frac{1}{2}\Delta^2t^2\right)$.

At first, we fitted all the ZF- and LF-spectra using a common $A_{\rm BG}$ over the whole temperature range and common, *i.e.* $H_{\rm LF}$-independent, Δ_i and ν ($\nu_1 = \nu_2$) at each temperature using eqn (3). Then, since both $A_{\rm KT1}$ and $A_{\rm KT2}$ were found to be approximately temperature-independent, we finally used common $A_{\rm KT1}$ and $A_{\rm KT2}$ for fitting the ZF- and LF-spectra. Here, Δ corresponds to a spin–spin relaxation rate ($1/T_2$), while ν corresponds to a combination of the muon hop rate and the nuclear spin-lattice relaxation rate ($1/T_1$).

3.3 Nature of diffusion in the three samples

3.3.1 ap-MgH_2. Fig. 4(a) shows the temperature dependence of the pressure (p) in the cell. As temperature increases from 350 K, p suddenly starts to increase at around 670 K and levels off to a constant value at 700 K due to a hydrogen desorption reaction with a temperature width ($\delta T_{\rm d}$) of 24.7 K. The desorption temperature for ap-MgH_2 is estimated to be $T_{\rm d}^{\rm mid} = 677.7(5)$ K, at which p is 50% of the value at 700 K, *i.e.* $p_{\rm max}$. We define $\delta T_{\rm d}$ as $\delta T_{\rm d} \equiv T(p = 0.9p_{\rm max}) - T(p = 0.1p_{\rm max})$. The desorption reaction is thus confirmed to occur very suddenly, as already reported.[21,22]

Concerning the μ^+SR parameters, both Δ_1 and Δ_2 decrease slightly with increasing temperature, but are roughly temperature independent up to $T_{\rm d}$, below which Δ_1 of the dominant $A_{\rm KT1}$ signal ranges between 0.33 and 0.31 μs^{-1} (equivalent to 3.8–3.6 Oe) and Δ_2 of the smaller $A_{\rm KT2}$ signal varies between 0.13 and 0.12 μs^{-1} (equivalent to 1.5–1.3 Oe) [Fig. 4(b)]. Above $T_{\rm d}$, Δ abruptly drops down to $\sim$0.07 μs^{-1} (equivalent to 0.8 Oe), as the $A_{\rm KT2}$ signal merges into the $A_{\rm KT1}$ signal [Fig. 4(d)]. The presence of the two $A_{\rm KT}$ signals below $T_{\rm d}^{\rm mid}$ suggests that about 30% of the implanted muons are located outside of the one-dimensional channel along the *c*-axis (Fig. 1), but still in the sample.

In addition, ν is very small and almost temperature independent up to around 670 K, but leaps up to $\sim$0.26 μs^{-1} at 700 K and increases with further increasing temperature [Fig. 4(c)]. Based on the $p(T)$ curve, MgH_2 fully decomposes into Mg and H_2 at 700 K. This indicates that the sudden decrease in Δ at $T_{\rm d}$ is most likely *not* caused by a motional narrowing behavior due to H and/or μ^+ diffusion, but by a change in the phase from MgH_2 to Mg due to the hydrogen desorption reaction, as proposed by macroscopic measurements.[12,26]

It should be noted that $\nu/\Delta_1 \sim 1/9$ at temperatures below $T_{\rm d}$. Furthermore, the magnitude of Δ_1 is about 1/2 of that determined by dipole field calculations with Dipelec,[58] *i.e.* $\Delta^{\rm calc}$ = 0.63–0.66 μs^{-1} (7.4–7.8 Oe) for an entirely static state. This suggests that μ^+ in MgH_2 is in a delocalized state even at room temperature, as predicted from the first principles calculations (see Fig. 1). However, since both Δ and ν are almost independent of temperature, H is most likely *not* mobile but rather vibrating at its equilibrium position. We will discuss this later in Section 4.1.

3.3.2 m-MgH_2. The $p(T)$ curve again shows a broad step-like transition at $T_{\rm d}^{\rm mid} = 546.0(8)$ K with $\delta T_{\rm d} = 56.4$ K [Fig. 4(e)], which is about twice as wide as $\delta T_{\rm d}$ for ap-MgH_2. This clearly shows that milling reduces $T_{\rm d}$ by about 145 K and makes the desorption reaction more moderate than that in ap-MgH_2.

The most significant difference between m-MgH_2 and ap-MgH_2 is found in the temperature dependence of Δ. That is, as seen in Fig. 4(f), although the magnitude of Δ_1 at 400 K is very close to that of Δ_1 for ap-MgH_2, Δ_2 is much larger than Δ_2 in ap-MgH_2. Since Δ_2 at 450 K is larger than $\Delta^{\rm calc}$, about 19% ($= \frac{A_{\rm KT2}}{A_{\rm KT1} + A_{\rm KT2}}$) of the implanted muons are thought to sit at fresh surfaces produced by milling, probably trapped by a dangling H^- bond. Furthermore, as temperature increases from 400 K, both Δ_1 and Δ_2 decrease monotonically up to around $T_{\rm d}^{\rm mid}$, and then decrease faster (larger $|{\rm d}\Delta/{\rm d}T|$), and are likely to level off to a constant value at around $T_{\rm d}^{\rm mid}$.

By contrast, as temperature increases from 400 K, ν decreases slightly with temperature up to $T_{\rm d}^{\rm mid}$, and then increases rapidly with temperature [Fig. 4(g)]. The steady decrease of Δ_1 and Δ_2 below 500 K, at which $p = 0$, suggests a motional narrowing behavior due to H diffusion in m-MgH_2. This is because μ^+ diffusion is temperature independent up to 700 K, based on the

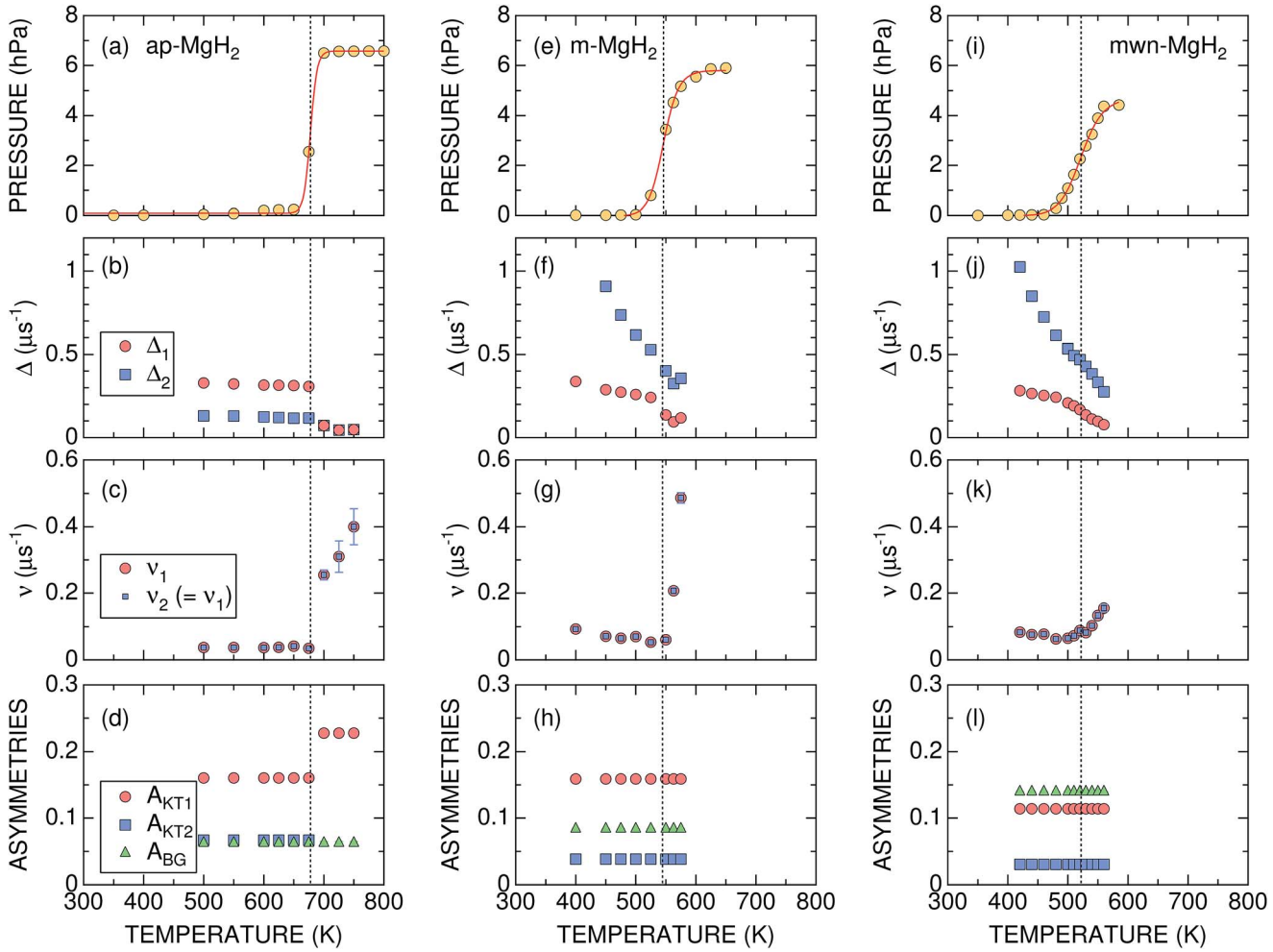

Fig. 4 The temperature dependences of the gas pressure and μ^+SR parameters for ap-, m-, and mwn-MgH_2 samples: (a), (e), and (i) gas pressure in the cell; (b), (f), and (j) the field distribution static widths (Δ_1 and Δ_2); (c), (g), and (k) the field fluctuation rates (ν_1 and ν_2); and (d), (h), and (l) the asymmetries (A_{KT1}, A_{KT2}, and A_{BG}). Except for pressure, the values shown were obtained by fitting the set of ZF- and LF-μ^+SR spectra with eqn (3). Dotted lines show T_d^{mid} determined from the $p(T)$ curve.

$\nu(T)$ curve in ap-MgH_2. The decrease in ν also indicates that both species are diffusing below T_d^{mid}. However, above T_d^{mid} the phase change from MgH_2 to Mg is the predominant reaction, resulting in a decrease in Δ and a rapid increase in ν.

3.3.3 mwn-MgH_2. According to the $p(T)$ curve in Fig. 4(i), H_2 starts to be released from mwn-MgH_2 at around 480 K, which stops at around 560 K, *i.e.* $T_d^{mid} = 522(2)$ K with $\delta T_d = 70.7$ K. Furthermore, p increases linearly with temperature above 480 K and levels off above 560 K. This shows that milling with Nb_2O_5 reduces T_d further by about 20 K.

The temperature dependences of Δ_1, Δ_2, and ν are similar to those for m-MgH_2, particularly below 450 K, at which $p = 0$. Above 450 K, both Δ_1 and Δ_2 decrease with temperature more rapidly, but ν increases slowly compared with ν in m-MgH_2. Overall results reveal that the changes in Δ and ν below 450 K are caused by H diffusion in MgH_2, while those above 450 K are induced by a gradual phase change from MgH_2 to Mg due to a hydrogen desorption reaction.

The ratio between A_{KT2} and $(A_{KT1} + A_{KT2})$ is about 20%, which is comparable to that of m-MgH_2 (19%). Thus, the surface structure of mwn-MgH_2 is most likely the same to that of m-MgH_2.

3.3.4 Asymmetries for the three samples. Since milling reduces the size of each MgH_2 particle, the packing density and/or amount of the sample in the cell is naturally different among the three samples. This results in a different p_{max} for the three samples, but we could estimate the amount of each sample in the cell by comparing the p_{max} with that of ap-MgH_2 ($p_{max}^{ap\text{-}MgH_2}$), defining the *normalized* p_{max} as $Np_{max} \equiv \hat{p_{max}}/p_{max}^{ap\text{-}MgH_2}$.

For samples exhibiting multiple asymmetries, each asymmetry is roughly proportional to the volume fraction of each phase. Since we used the same measurement setup for the three samples, the volume fraction (V_F) of the sample is given by

$$V_F = \frac{A_{KT1} + A_{KT2}}{A_{KT1} + A_{KT2} + A_{BG}}.$$

Therefore the *normalized* V_F, which is given by $NV_F \equiv \hat{V}_F^{ap\text{-}MgH_2}$, also provides a rough estimate for the amount of each sample. In fact, as seen in Fig. 5, a linear relationship

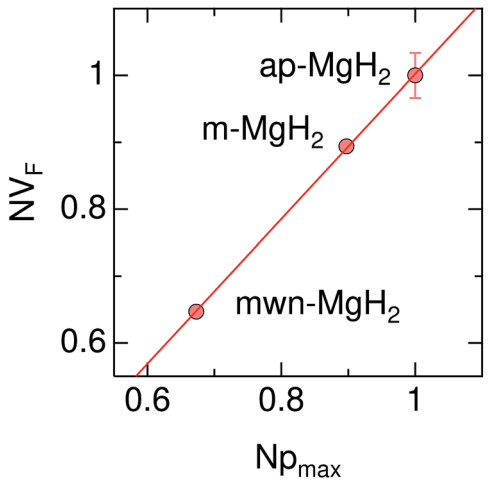

Fig. 5 The relationship between the normalized volume fraction of the sample (NV_F) and the normalized maximum pressure (Np_{max}) for the three MgH_2 samples. Here, the volume fraction of the sample is defined as $V_F = (A_{KT1} + A_{KT2})/(A_{KT1} + A_{KT1} + A_{BG})$. For NV_F, each V_F is divided by V_F for ap-MgH_2. p_{max} is the pressure at the highest temperature measured [see Fig. 4(a), (e), and (i)], and, for Np_{max}, each p_{max} is divided by p_{max} for ap-MgH_2.

between Np_{max} and NV_F demonstrates the reliability of the above explanation.

4 Discussion

4.1 Implanted muons in MgH_2

As predicted by first principles calculations, μ^+ is most likely in a delocalized state in a 1D channel of MgH_2 even at room temperature [see Fig. 6(a)]. This has been confirmed by a very recent negative muon (μ^-) spin rotation and relaxation experiment on ap-MgH_2.[59] That is, from the fixed position of μ^- captured on Mg, μ^-SR shows that $\Delta = 0.520(7)$ μs^{-1} [equivalent to 6.11(8) Oe], which is very close to the calculated value ($\Delta^{calc} = 0.5807$ μs^{-1}) at the Mg site in MgH_2. By contrast, the present μ^+SR shows that $\Delta \sim 0.3$ μs^{-1} [equivalent to 2.55 Oe] for MgH_2 below 400 K, while the calculated Δ in the 1D channel ranges between 0.629 and 0.664 μs^{-1} [equivalent to 7.39 and 7.80 Oe] [see Fig. 6(b)]. This clearly indicates that μ^+ is not immobile, but delocalized along the 1D channel.

Since ν for ap-MgH_2 is independent of temperature up to around 670 K, the delocalized state of μ^+ is not altered with temperature in the temperature range between 300 and 760 K, probably due to a very small energy barrier in the 1D channel [see Fig. 6(a)]. Nevertheless, the $\Delta(T)$ curves show a motional narrowing behavior below 550 K for m- and 500 K for mwn-MgH_2 samples. This means that the delocalized μ^+ feels a fluctuating H_{int} caused by H diffusion, which occurs even at temperatures for which $p = 0$. We wish to emphasize again that μ^+ *feels* a static and/or dynamic nuclear field formed by ^{1}H in MgH_2, but does not sense it in Mg due to dilute concentration of H. Consequently, μ^+SR clearly detects H diffusion in MgH_2, where a desorption reaction does not occur, although it would be difficult to reliably estimate the diffusion coefficient of H under this circumstance, *i.e.* the observation of mobile H from a delocalized viewpoint.

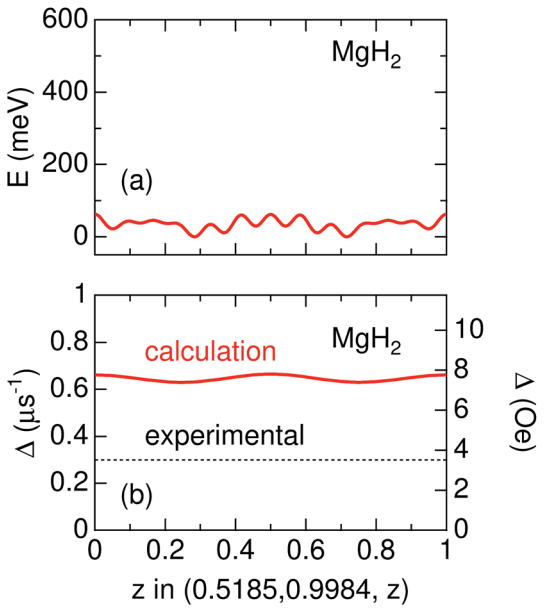

Fig. 6 The variation of (a) electrostatic potential (E) predicted by first principles calculations and (b) Δ estimated by dipole field calculations as a function of z along the line (0.5185, 0.9984, z) in MgH_2. In (a), the difference between the maximum E and minimum E is about 60 meV, suggesting that the μ^+ is in a delocalized state, particularly at high temperatures. Since the zero-point energy of μ^+ is expected to be about 600 meV (see in the text), the range of the vertical axis in (a) is between −50 and 600 meV.

4.2 Activation energy

When ν is due only to ion diffusion, the $\nu(T)$ curve is well explained by a thermal activation process. However, the ν values in the three MgH_2 samples are not simply determined by a single diffusion process, as mentioned above. Hence, Fig. 7 shows instead the relationship between $1/\Delta$ and inverse temperature. The activation energy (E_a) for $1/\Delta_1$ in m-MgH_2 and mwn-MgH_2 is estimated to be 0.045(2) and 0.040(2) eV, respectively, while E_a for $1/\Delta_2$ in m-MgH_2 and mwn-MgH_2 is 0.155(3) and 0.134(3) eV, respectively. This means that E_a values for m-MgH_2 are similar to those for mwn-MgH_2. These values are comparable to the diffusion activation energy for MgH_2 predicted by first principles calculations.[33,34] In contrast, past ^{1}H-NMR measurements on $1/T_1$ in ap-MgH_2 revealed that $E_a = 1.72$ eV in the temperature range between 500 and 666 K,[30] but no data for m- and mwn-MgH_2 were reported.

Therefore, the milling is found to enhance H diffusion in MgH_2 through the formation of fresh surfaces. Such an enhancement leads to a decrease in T_d. However, since there are no clear differences in the μ^+SR parameters below 500 K between m-MgH_2 and mwn-MgH_2, the role of Nb_2O_5 in reducing T_d is still not clarified. In order to further understand the dynamic behavior in MgH_2, we definitely need to separate the contribution of μ^+ diffusion from the μ^+SR data. For this purpose, we have initiated a negative muon spin rotation and relaxation experiment on MgH_2,[59] because μ^- is captured by Mg nuclei and thus μ^-SR provides information on H_{int} from a fixed viewpoint.

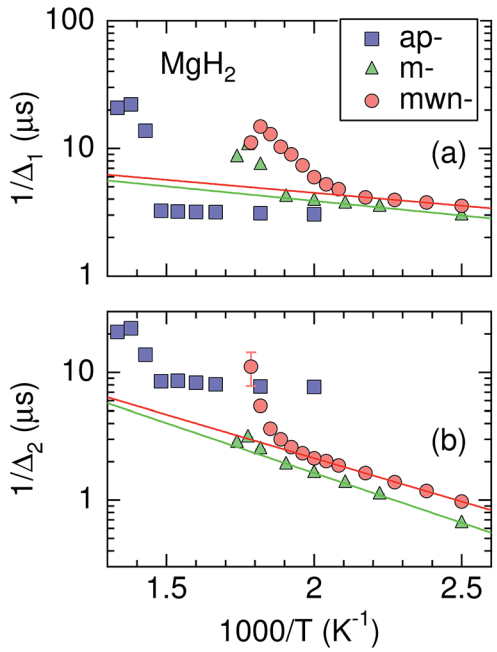

Fig. 7 The relationship between Δ and pressure (p) for the three MgH_2 samples. Solid lines represent a fit obtained using the Arrhenius law $\Delta = \Delta_0 \exp(-E_a/k_BT)$ at temperatures below 500 K for m-MgH_2 and below 450 K for mwn-MgH_2. Here Δ_0 is the frequency factor, E_a is the activation energy, and k_B is Boltzmann constant.

5 Conclusions

We have carried out an "*in situ*" μ^+SR experiment on MgH_2 to measure the pressure in the sample cell in parallel to the μ^+SR spectrum under static conditions. The motivation behind this experiment is to clarify the role of H diffusion in solid MgH_2 in determining the hydrogen desorption temperature (T_d). This is, to our knowledge, the first *in situ* experiment to observe such a reaction in solids with μ^+SR.

We have found that, as T_d is decreased by milling or milling with Nb_2O_5, the diffusive behavior of H in MgH_2 is observed well below T_d, where the Mg phase does not exist. This suggests that rapid H diffusion in MgH_2 is one of the key factors to reduce T_d, since the liberated H from the MgH_2 phase should be removed through the surface with H diffusion.

Finally, we wish to emphasize that *in situ* μ^+SR experiments will provide clear insights into many reaction mechanisms through measurements of ion diffusion in solids and its thermal activation energy. This is because many reactions are often accompanied by mass transport in solids.

Author contribution statement

J.S. conceived the experiments. I.U. prepared and performed the experiments at ISIS together with J.S., H.N., Y.H., O.K.F., M. Månsson and the local ISIS support from S.P.C. J.S., H.N., and I.U. joined the μ^+SR experiments at J-PARC and A.K. assisted them. J.S., H.N., T.N., E.J.A., and J.H.B. performed the μ^+SR experiments at TRIUMF. M. Matsumoto and I.U. prepared the m- and mwn-MgH_2 samples. K.M. performed the first principles calculations. J.S. analyzed the data and created the first draft with I.U. J.H.B. and M. Månsson edited the draft, and all authors reviewed the manuscript in several steps.

Conflicts of interest

There are no conflicts to declare.

Acknowledgements

We thank the staff of TRIUMF, J-PARC, and ISIS for help with the μ^+SR experiments with the following proposal numbers: M1175, 2012A0089, 2013A0019, RB1510262, and RB1520259. We are particularly grateful to Chris Goodway, Paul McIntyre, Adam Sears, and Mark Kibble of the pressure and furnace group at ISIS, for their support that was essential for a successful experiment. J.S. specially thanks Dr Shinichi Towata of the Aichi Synchrotron Radiation Center for his encouragement to this work. M. Månsson and O.F.K. are partly supported by a Marie Skłdowska Curie Action, International Career Grant through the European Commission and Swedish Research Council (VR), Grant No. INCA-2014-6426 as well as a VR neutron project grant (BIFROST, Dnr. 2016-06955). Further support was also granted by the Carl Tryggers Foundation for Scientific Research (CTS-16:324 and CTS-17:325). This work was supported by the Ministry of Education, Culture, Sports, Science and Technology (MEXT) of Japan, KAKENHI Grant no. JP23108003 and JP26108722 and Japan Society for the Promotion Science (JSPS) KAKENHI Grant no. JP26286084 and JP18H01863.

References

1 G. M. Kalvius, D. R. Noakes and O. Hartmann, in *Handbook on the Physics and Chemistry of Rare Earths*, ed. K. A. Gschneidner, J. L. Eyring and G. H. Lander, North-Holland, Amsterdam, 2001, vol. 32, ch. 206, pp. 55–451.
2 A. Yaouanc and P. D. de Réotier, in *Muon Spin Rotation, Relaxation, and Resonance, Application to Condensed Matter*, Oxford, New York, 2011.
3 P. J. C. King, R. de Renzi, S. P. Cottrell, A. D. Hillier and S. F. J. Cox, *Phys. Scr.*, 2013, **88**, 068502.
4 Y. Miyake, K. Shimomura, N. Kawamura, A. Koda, P. Strasser, K. M. Kojima, H. Fujimori, S. Makimura, Y. Ikedo, Y. Kobayashi, J. Nakamura, Y. Oishi, S. Takeshita, T. Adachi, A. D. Pant, H. Okabe, S. Matoba, M. Tampo, M. Hiraishi, K. Hamada, S. Doiuchi, W. Higemoto, T. U. Ito and R. Kadono, *JPS Conf. Proc.*, 2018, **21**, 011054.
5 S. Giblin, S. Cottrell, P. King, S. Tomlinson, S. Jago, L. Randall, M. Roberts, J. Norris, S. Howarth, Q. Mutamba, N. Rhodes and F. Akeroyd, *Nucl. Instrum. Methods Phys. Res., Sect. A*, 2014, **751**, 70.
6 A. D. Hillier, M. Aramini, P. J. Baker, A. Berlie, P. K. Biswas, S. P. Cottrell, K. Ishida, T. Loe, J. S. Lord, D. E. Pooley, F. L. Pratt, N. J. Rhodes, R. J. da Silva Afonso, M. T. F. Telling and K. Yokoyama, *JPS Conf. Proc.*, 2018, **21**, 011055.

7 K. M. Kojima, T. Murakami, Y. Takahashi, H. Lee, S. Y. Suzuki, A. Koda, I. Yamauchi, M. Miyazaki, M. Hiraishi, H. Okabe, S. Takeshita, R. Kadono, T. Ito, W. Higemoto, S. Kanda, Y. Fukao, N. Saito, M. Saito, M. Ikeno, T. Uchida and M. M. Tanaka, *J. Phys.: Conf. Ser.*, 2014, **551**, 012063.
8 T. Noritake, M. Aoki, S. Towata, Y. Seno, Y. Hirose, E. Nishibori, M. Takata and M. Sakata, *Appl. Phys. Lett.*, 2002, **81**, 2008–2010.
9 L. Schlapbach and A. Züttel, *Nature*, 2001, **414**, 353.
10 J. F. Stampfer, C. E. Holley and J. F. Suttle, *J. Am. Chem. Soc.*, 1960, **82**, 3504–3508.
11 B. Sakintuna, F. Lamari-Darkrim and M. Hirscher, *Int. J. Hydrogen Energy*, 2007, **32**, 1121–1140.
12 J.-C. Crivello, B. Dam, R. V. Denys, M. Dornheim, D. M. Grant, J. Huot, T. R. Jensen, P. de Jongh, M. Latroche, C. Milanese, D. Milčius, G. S. Walker, C. J. Webb, C. Zlotea and V. A. Yartys, *Appl. Phys. A: Mater. Sci. Process.*, 2016, **122**, 97.
13 Y. Wang and Y. Wang, *Prog. Nat. Sci.: Mater. Int.*, 2017, **27**, 41–49.
14 P. Tessier and E. Akiba, *J. Alloys Compd.*, 1999, **293–295**, 400–402.
15 G. Liang, J. Huot, S. Boily, A. V. Neste and R. Schulz, *J. Alloys Compd.*, 1999, **292**, 247–252.
16 J.-L. Bobet, B. Chevalier, M. Song, B. Darriet and J. Etourneau, *J. Alloys Compd.*, 2002, **336**, 292–296.
17 G. Barkhordarian, T. Klassen and R. Bormann, *Scr. Mater.*, 2003, **49**, 213–217.
18 G. Barkhordarian, T. Klassen and R. Bormann, *J. Alloys Compd.*, 2004, **364**, 242–246.
19 G. Barkhordarian, T. Klassen and R. Bormann, *J. Alloys Compd.*, 2006, **407**, 249–255.
20 N. Hanada, T. Ichikawa and H. Fujii, *J. Alloys Compd.*, 2007, **446–447**, 67–71.
21 H. Reule, M. Hirscher, A. Weißhardt and H. Kronmüller, *J. Alloys Compd.*, 2000, **305**, 246–252.
22 N. Hanada, T. Ichikawa, S.-I. Orimo and H. Fujii, *J. Alloys Compd.*, 2004, **366**, 269–273.
23 N. Hanada, T. Ichikawa and H. Fujii, *J. Alloys Compd.*, 2005, **404–406**, 716–719.
24 N. Hanada, T. Ichikawa, S. Hino and H. Fujii, *J. Alloys Compd.*, 2006, **420**, 46–49.
25 K. Alsabawi, E. Gray and C. Webb, *Int. J. Hydrogen Energy*, 2019, **44**, 2976–2980.
26 M. Martin, C. Gommel, C. Borkhart and E. Fromm, *J. Alloys Compd.*, 1996, **238**, 193–201.
27 J. Töpler, H. Buchner, H. Säufferer, K. Knorr and W. Prandl, *J. Less-Common Met.*, 1982, **88**, 397–404.
28 V. P. Zhdanov, A. Krozer and B. Kasemo, *Phys. Rev. B: Condens. Matter Mater. Phys.*, 1993, **47**, 11044–11048.
29 E. Evard, I. Gabis and V. Yartys, *Int. J. Hydrogen Energy*, 2010, **35**, 9060–9069.
30 R. L. Corey, T. M. Ivancic, D. T. Shane, E. A. Carl, R. C. Bowman, J. M. Bellosta von Colbe, M. Dornheim, R. Bormann, J. Huot, R. Zidan, A. C. Stowe and M. S. Conradi, *J. Phys. Chem. C*, 2008, **112**, 19784–19790.
31 A. J. Du, S. C. Smith and G. Q. Lu, *J. Phys. Chem. C*, 2007, **111**, 8360–8365.
32 X. Yao, Z. Zhu, H. Cheng and G. Lu, *J. Mater. Res.*, 2008, **23**, 336–340.
33 S. Hao and D. S. Sholl, *Appl. Phys. Lett.*, 2008, **93**, 251901.
34 M. S. Park, A. Janotti and C. G. Van de Walle, *Phys. Rev. B: Condens. Matter Mater. Phys.*, 2009, **80**, 064102.
35 S. Hao and D. S. Sholl, *J. Phys. Chem. Lett.*, 2010, **1**, 2968–2973.
36 E. German and R. Gebauer, *J. Phys. Chem. C*, 2016, **120**, 4806–4812.
37 J. Sugiyama, K. Mukai, Y. Ikedo, H. Nozaki, M. Månsson and I. Watanabe, *Phys. Rev. Lett.*, 2009, **103**, 147601.
38 A. S. Powell, J. S. Lord, D. H. Gregory and J. J. Titman, *J. Phys. Chem. C*, 2009, **113**, 20758–20763.
39 J. Sugiyama, H. Nozaki, M. Harada, K. Kamazawa, O. Ofer, M. Månsson, J. H. Brewer, E. J. Ansaldo, K. H. Chow, Y. Ikedo, Y. Miyake, K. Ohishi, I. Watanabe, G. Kobayashi and R. Kanno, *Phys. Rev. B: Condens. Matter Mater. Phys.*, 2011, **84**, 054430.
40 P. J. Baker, I. Franke, F. L. Pratt, T. Lancaster, D. Prabhakaran, W. Hayes and S. J. Blundell, *Phys. Rev. B: Condens. Matter Mater. Phys.*, 2011, **84**, 174403.
41 J. Sugiyama, H. Nozaki, M. Harada, K. Kamazawa, Y. Ikedo, Y. Miyake, O. Ofer, M. Månsson, E. J. Ansaldo, K. H. Chow, G. Kobayashi and R. Kanno, *Phys. Rev. B: Condens. Matter Mater. Phys.*, 2012, **85**, 054111.
42 M. Månsson and J. Sugiyama, *Phys. Scr.*, 2013, **88**, 068509.
43 A. S. Powell, Z. Stoeva, J. S. Lord, R. I. Smith, D. H. Gregory and J. J. Titman, *Phys. Chem. Chem. Phys.*, 2013, **15**, 816–823.
44 J. Sugiyama, H. Nozaki, I. Umegaki, K. Mukai, K. Miwa, S. Shiraki, T. Hitosugi, A. Suter, T. Prokscha, Z. Salman, J. S. Lord and M. Månsson, *Phys. Rev. B: Condens. Matter Mater. Phys.*, 2015, **92**, 014417.
45 I. Umegaki, S. Kawauchi, H. Sawada, H. Nozaki, Y. Higuchi, K. Miwa, Y. Kondo, M. Månsson, M. Telling, F. C. Coomer, S. P. Cottrell, T. Sasaki, T. Kobayashi and J. Sugiyama, *Phys. Chem. Chem. Phys.*, 2017, **19**, 19058–19066.
46 J. Sugiyama, I. Umegaki, T. Uyama, R. M. L. McFadden, S. Shiraki, T. Hitosugi, Z. Salman, H. Saadaoui, G. D. Morris, W. A. MacFarlane and R. F. Kiefl, *Phys. Rev. B: Condens. Matter Mater. Phys.*, 2017, **96**, 094402.
47 I. Umegaki, H. Nozaki, M. Harada, Y. Higuchi, T. Noritake, M. Matsumoto, S. i. Towata, E. J. Ansaldo, J. H. Brewer, A. Koda, Y. Miyake and J. Sugiyama, *J. Phys.: Conf. Ser.*, 2014, **551**, 012036.
48 J. Sugiyama, *J. Phys. Soc. Jpn.*, 2016, **85**, 091012.
49 A. Suter and B. Wojek, *Phys. Procedia*, 2012, **30**, 69–73.
50 K. Miwa and A. Fukumoto, *Phys. Rev. B: Condens. Matter Mater. Phys.*, 2002, **65**, 155114.
51 R. Kadono, K. Shimomura, K. H. Satoh, S. Takeshita, A. Koda, K. Nishiyama, E. Akiba, R. M. Ayabe, M. Kuba and C. M. Jensen, *Phys. Rev. Lett.*, 2008, **100**, 026401.
52 J. Sugiyama, Y. Ikedo, T. Noritake, O. Ofer, T. Goko, M. Månsson, K. Miwa, E. J. Ansaldo, J. H. Brewer, K. H. Chow and S.-I. Towata, *Phys. Rev. B: Condens. Matter Mater. Phys.*, 2010, **81**, 092103.

53 J. H. Brewer, S. R. Kreitzman, D. R. Noakes, E. J. Ansaldo, D. R. Harshman and R. Keitel, *Phys. Rev. B: Condens. Matter Mater. Phys.*, 1986, **33**, 7813–7816.
54 K. Nishiyama, S. Nishiyama and W. Higemoto, *Phys. B*, 2003, **326**, 41–45.
55 Y. Itoh and R. Kado, *J. Phys. Soc. Jpn. Conf. Proc.*, 2014, **1**, 012013.
56 R. S. Hayano, Y. J. Uemura, J. Imazato, N. Nishida, T. Yamazaki and R. Kubo, *Phys. Rev. B: Condens. Matter Mater. Phys.*, 1979, **20**, 850–859.
57 R. Kubo and T. Toyabe, in *Magnetic Resonance and Relaxation*, ed. R. Bline, North-Holland, Amsterdam, 1996.
58 K. M. Kojima, J. Yamanobe, H. Eisaki, S. Uchida, Y. Fudamoto, I. M. Gat, M. I. Larkin, A. Savici, Y. J. Uemura, P. P. Kyriakou, M. T. Rovers and G. M. Luke, *Phys. Rev. B: Condens. Matter Mater. Phys.*, 2004, **70**, 094402.
59 J. Sugiyama, I. Umegaki, H. Nozaki, W. Higemoto, K. Hamada, S. Takeshita, A. Koda, K. Shimomura, K. Ninomiya and M. K. Kubo, *Phys. Rev. Lett.*, 2018, **121**, 087202.